Selection for Size in Molecular Self-Assembly Drives the *De Novo* Evolution of a Molecular Machine

Zena Hadjivasiliou[1,2,3,4,5,*] and Karsten Kruse[5,6,7,†]

[1]*London Centre for Nanotechnology, University College London, London, United Kingdom*
[2]*Department of Physics and Astronomy, University College London, London, United Kingdom*
[3]*Institute for the Physics of Living Systems, University College London, London, United Kingdom*
[4]*Mathematical and Physical Biology Laboratory, The Francis Crick Institute, London, United Kingdom*
[5]*Department of Biochemistry, University of Geneva, Geneva, Switzerland*
[6]*NCCR for Chemical Biology, University of Geneva, Geneva, Switzerland*
[7]*Department of Theoretical Physics, University of Geneva, Geneva, Switzerland*

(Received 13 June 2022; accepted 27 September 2023; published 14 November 2023)

The functioning of machines typically requires a concerted action of their parts. This requirement also holds for molecular motors that drive vital cellular processes and imposes constraints on their conformational changes as well as the rates at which they occur. It remains unclear whether, during evolution, features required for functional molecular machines can emerge simultaneously or require sequential adaptation to different selection pressures. We address this question by theoretically analyzing the evolution of filament treadmilling. This process refers to the self-assembly of linear polymers that grow and shrink at equal rates at their opposite ends. It constitutes a simple biological molecular machine that is involved in bacterial cell division and requires that several conditions are met. In our simulation framework, treadmilling emerges as a consequence of selecting for a target average polymer length. We discuss why other forms of assembly dynamics, which also reach the imposed target length, do not emerge in our simulations. Our work shows that complex molecular functions can evolve *de novo* under selection for a single physical feature.

DOI: 10.1103/PhysRevLett.131.208402

Well-crafted molecular machines underlie functions that are fundamental to life, such as DNA replication or transport of cellular cargo [1,2]. These processes involve molecular motors that produce directional motion. The functioning of molecular motors has been characterized in detail from both a biological and a physical perspective. In particular, physics imposes that the generation of directional motion at a molecular level requires structural polarity and a departure from thermodynamic equilibrium [3]. In contrast, we still understand little about the selection forces that could drive the evolution of molecular motors.

The broader question of how complex organs and biological processes evolve through natural selection has puzzled evolutionary biologists since Darwin [4]. It is often assumed that complexity emerges incrementally so that different features required for an elaborate function are acquired sequentially due to different selection pressures [5,6].

In this Letter, we consider the *de novo* evolution of molecular motors as a basis to explore the evolution of complex functions from simpler components. We use stochastic simulations to study how molecular self-assembly can evolve to perform directional motion. A simple way to achieve this is through treadmilling, a process in which filamentous molecular aggregates grow at one end and shrink at the other, on average at equal rates. This behavior has been reported for actin filaments [7] and microtubules [8,9] and plays a crucial role in bacteria [10–15]. When linked to other structures, treadmilling can generate mechanical stress similar to other molecular motors.

We develop a framework to study molecular self-assembly in the context of evolution, and explore the emergence of treadmilling. This is nontrivial as treadmilling requires several conditions to be simultaneously met (see below). As such, it is not obvious whether treadmilling can evolve *de novo* as a response to a single selection pressure or if the different properties required for treadmilling must evolve sequentially. Our results show that selection for filaments of fixed average length is sufficient.

To study the evolution of treadmilling, one must consider events on two timescales. First, the timescale of filament assembly, which is governed by the rates of subunit attachment and detachment. Second, the timescale of

evolution on which the rates of filament assembly change by mutation and selection. In this work, we assume that evolution occurs on longer timescales than filament assembly so that filaments reach steady state between mutation events. Selection thus acts on the steady state.

Filament assembly dynamics and conditions for treadmilling.—On the molecular level, treadmilling requires the assembling subunits to exist in at least two states with different binding affinities [16]. In detailed descriptions of filament dynamics, three states are widely used [17–19]. In biological filaments, these states correspond to subunits bound to different nucleotides. Typically, their binding affinity is larger when bound to a nucleoside tri-phosphate (NTP) and lower when bound to a nucleoside di-phosphate (NDP) [20–22]. In the treadmilling state, NTP-bound subunits bind at one filament end and subsequently experience NTP hydrolysis. Eventually, NDP-bound subunits unbind at the opposite filament end. Growth at one and shrinkage at the opposite end confers polarity to the filament, and the spatial separation of attachment and detachment reflects the nonequilibrium nature of this process. Treadmilling thus fulfills the minimal requirements for the operation of a molecular motor [3].

We represent a filament by a dynamic linear lattice [16], Fig. 1(a). Each lattice site stands for a single subunit in one of two states. The two states are denoted by H and L for high and low binding affinity, respectively. Subunits within the lattice switch between the two states at rate ω_{HL} from H to L and at rate ω_{LH} for the reverse transition. We denote the two ends of the lattice by $+$ and $-$ such that the largest attachment rate occurs at the plus end. The various rates of attachment and detachment at the two ends are denoted by $k_a^H(+)$, $k_a^H(-)$, $k_d^H(+)$, and $k_d^H(-)$ for subunits in state H and similarly for subunits in state L, Fig. 1(a). Subunits not attached to the lattice form a reservoir, such that the attachment rates are constant. Finally, we assume that the attachment and detachment rates only depend on the state of the subunit that is added to or removed from the lattice. Therefore, the equilibrium constants are equal at the two ends, $K_H \equiv k_a^H(+)/k_d^H(+) = k_a^H(-)/k_d^H(-)$ and similarly for subunits in state L. This assumption is not always true, e.g. [23], see also SM. By definition, H and L implies $K_H > K_L$.

Treadmilling can occur in this description if several conditions are met [16]: (i) $K_H > 1$, (ii) $K_L < 1$ such that H subunits are on average added to the lattice, whereas L subunits are removed on average, and (iii) $\omega_{HL} \gg \omega_{LH}$ so that bound H subunits are more likely to transition to bound L subunits than vice versa. It follows from (i)-(iii) that the probability for a site to be in state H or L depends on the time that has passed since its incorporation into the lattice. Consequently, the probability of the site at the minus end to be in state H or L and thus also the corresponding net detachment rate, $k_d(-)$, effectively depends on the lattice length [16].

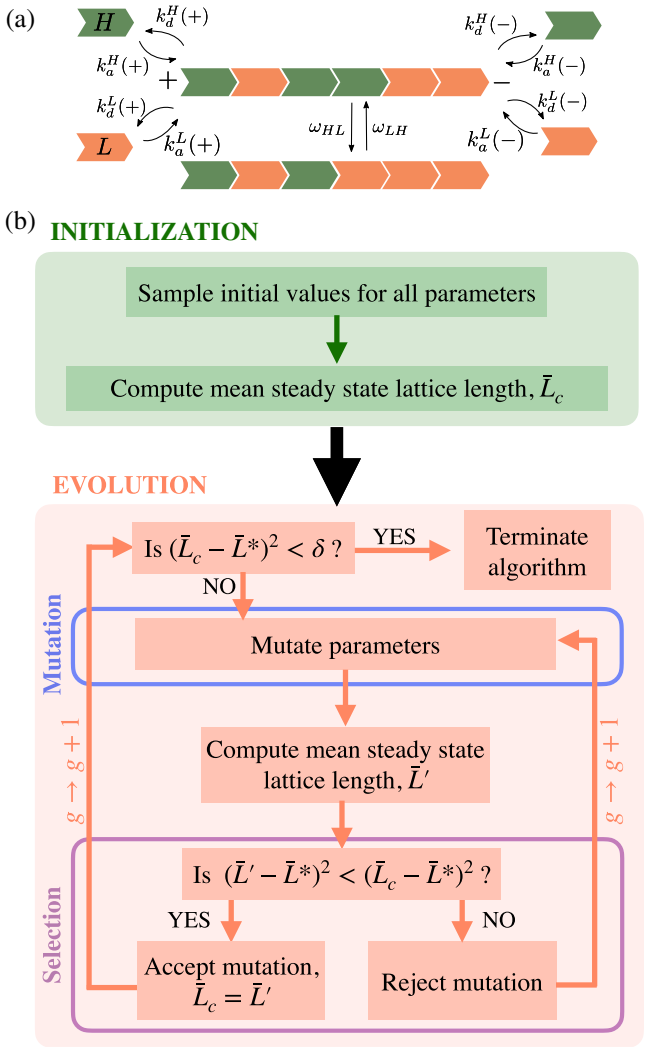

FIG. 1. Schematic diagram of filament dynamics and evolution algorithm. (a) A two-state model for active filaments. Subunits are in one of two states denoted by H for high affinity (green blocks) and L for low affinity (orange blocks), respectively. Subunits are added and removed from the two filament ends, $+$ and $-$, at rates given in the figure. Transitions between the two subunit states within a filament occur at rates ω_{HL} and ω_{LH}. (b) Diagram of the evolution algorithm employed in this study. We initiate simulations by randomly sampling the parameters shown in (a) and computing the steady state mean lattice length for the current parameter set, $\bar{L}_c$. This is followed by an evolution loop where parameters are mutated and mutations are accepted if the steady state mean lattice length, $\bar{L}'$, is closer to the target length, $\bar{L}^*$, than that before mutation. Each loop of mutation and selection constitutes a generation, g. The algorithm is terminated when the current lattice steady state mean length is within a predefined distance from the target length.

Treadmilling requires two further conditions to be fulfilled: The net attachment rate at the plus end, $k_a(+)$, and the maximal and minimal net detachment rates at the minus end, $k_d^{\min}(-)$ and $k_d^{\max}(-)$ must satisfy (iv) $k_a(+) > k_d^{\min}(-)$ and (v) $k_a(+) < k_d^{\max}(-)$. These conditions imply

that, on average, plus-end growth is between the minimal and maximal shrinkage at the minus end.

It follows from the considerations above that filament treadmilling requires the coordination between several independent molecular rates. Importantly, starting from random values for these rates, it is not obvious whether conditions (i)-(v) can all be satisfied as a result of evolution under a single selection pressure or must evolve independently in a sequential manner and driven by different selection pressures.

Evolution algorithm.—In our evolution algorithm, a mutation consists of changing the parameter values that govern the assembly dynamics, Fig. 1(b). The rate changes are intended to capture structural changes of the subunits due to genetic modifications. For selection, we considered the average length in steady state. A generation in our evolution scheme encompasses a single round of mutation and selection: following a change of the parameter values (mutation), we determined the corresponding average length, $\bar{L}'$, and accepted the mutation (selection) if the average length was closer to the target value, $\bar{L}^*$, than for the previous parameters, Fig. 1(b). This algorithm mirrors an adaptive dynamics approach, where evolution occurs in a large, asexual population and is fast so that new mutations vanish or invade to replace the resident quickly [24]. More details on our implementation of the mutation process and evolution algorithm are given in the Supplemental Material [25] which includes Refs. [23,26].

For a given set of parameter values, we obtained the average length in steady state through stochastic simulations of the discrete lattice dynamics employing the Gillespie scheme. To limit simulation time and keep track of the lattice ends, we assumed a minimum lattice length of 2 subunits and a maximum lattice length of 2000 subunits, which was much larger than our evolutionary target average length $\bar{L}^* = 200$. When the maximum length was reached, no further binding was allowed. We ran simulations for 10^6 s of simulated time before sampling the lattice length every 20 simulation steps until 10^6 samples were obtained. The average of the sampled lengths was taken as an estimate of the average steady state length.

We start our evolution algorithm from random initial values for the different rates, Fig. 1(b). For the 204 evolution processes we performed, none exhibited treadmilling at the initial state suggesting that the parameter region allowing treadmilling has a measure that is at least 2 orders of magnitude smaller compared to the region of nontreadmilling parameter values. In addition, the mean lattice length characterizing the initial stage of evolution, either diverged or was just a few subunits long, see Supplemental Material [25] and Fig. S1. We assumed mutation-selection balance was reached and terminated the evolution process when the difference between the current, $\bar{L}_c$, and target mean length satisfied $(\bar{L}_c - \bar{L}^*)^2 < \delta$ with $\delta = (\bar{L}^*/20)^2$, Fig. 1(b).

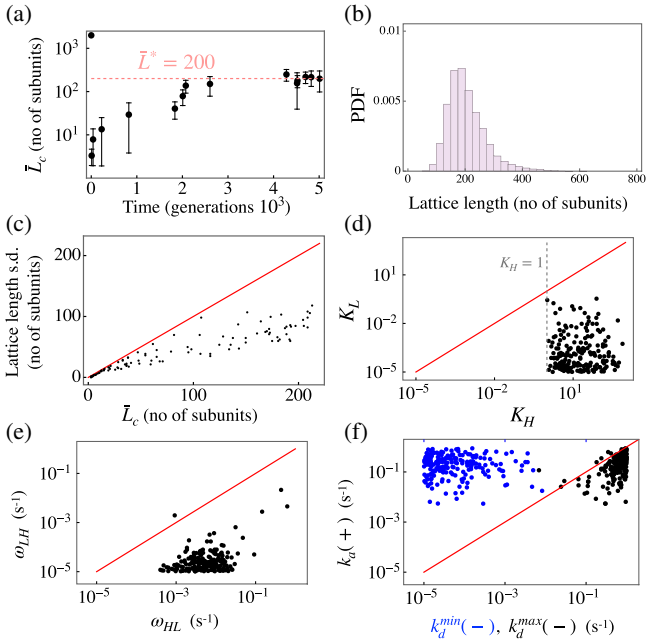

FIG. 2. Lattices converge to target length and evolved lattices are polar. (a) Example of current mean length, $\bar{L}_c$, in steady state versus evolutionary generation time. Bars indicate standard deviation of the steady-state length distribution. A single generation, consists of a round of mutation and selection in our evolution algorithm, Fig. 1(b). An error bar is absent for the initial parameter values as they lead to a diverging lattice which rests at the upper limit of 2000 subunits. More instances shown in Fig. S1 [25]. (b) Example steady-state length distribution at mutation-selection balance. (c) Standard deviation versus mean length, $\bar{L}_c$. Data are pooled for all evolution steps across all 204 simulated evolution experiments. (d) Evolved affinity of L subunits versus that of the H subunits. (e) Evolved rate at which H subunits transform into L subunits, ω_{HL}, versus the rate of the inverse transformation, ω_{LH}. (f) Evolved net subunit attachment rate, $k_a(+)$, at the plus- versus evolved minimal net detachment rate at the minus-end, $k_d^{\min}(-)$ (blue) and evolved maximal net detachment rate at the minus end, $k_d^{\max}(-)$ (black). Data in (d)–(f) obtained at mutation-selection balance across 204 simulated evolution experiments. Red lines in (d)–(f) indicate the line $x = y$.

Filaments evolve target length and treadmilling.—In all cases, the average lattice length converged to $\bar{L}^*$, Fig. 2(a). The convergence process was typically biphasic: first the average length decreased to just a few subunits. The corresponding length distribution was exponential. Subsequently, the average length gradually increased. The corresponding length distributions remained unimodal, Fig. 2(b), but with a reduced standard deviation compared to the mean length, Fig. 2(c).

In all our simulated evolution experiments ($N = 204$), a substantial difference evolved between the equilibrium constants K_H and K_L. In fact, $K_H > 1$ and $K_L < 1$ for all evolved states, which thus satisfied conditions (i) and (ii) required for treadmilling, Fig. 2(d). With one exception, the conversion rate ω_{HL} from the H to the L state was larger

by at least an order of magnitude relative to the opposite process, Fig. 2(e), satisfying condition (iii). In addition, all evolved states exhibited polarity, such that $k_a(+) > k_d^{\min}(-)$ satisfying condition (iv), Fig. 2(f). Together, these results show that selection for an average filament length can lead to the simultaneous evolution of subunits that have strikingly different affinities for the assembly, form polar lattices, and have different transition rates between the two states of bound subunits.

To explore whether the evolved lattices indeed exhibit treadmilling, we first measured at mutation-selection balance the steady state position-dependent probability for a site to be in the H state. This probability decreased exponentially from the plus end until about twice the target lattice length, Fig. 3(a) (also see Ref. [16]). In steady state, the gradient in the H-state probability led to a net detachment rate that increased monotonically with the lattice length, Figs. 3(b) and 3(c) and [25] for calculation details.

We next computed the average shrinkage rate of lattices at the minus end at the mutation selection balance, see details in the Supplemental Material [25]. With no exception, this rate was equal to the rate at which lattices grew at the plus end, confirming that all evolved lattices treadmilled, Fig. 3(d). The position and composition of an evolved lattice in steady state is shown in Fig. 3(e), highlighting that evolved lattices perform directed motion. Finally, for steady state lattices at mutation-selection balance, $\omega_{HL} - \omega_{LH}$ increased as a power law with $k_a^H(+) - k_d^H(+)$ so that $\omega_{HL} - \omega_{LH} = \beta(k_a^H(+) - k_d^H(+))^q$, Fig. 3(f). In addition, varying the target length in the evolution algorithm revealed that, while q did not change noticeably, β decreased with $\bar{L}^*$, Fig. 3(g) and Fig. S2 [25]. Therefore, evolution in our algorithm regulates the ratio between the effective transition rate from a high to a low affinity bound subunit, $\omega_{HL} - \omega_{LH}$, and the effective attachment rate of the high affinity subunit at the plus end, $k_a^H(+) - k_d^H(+)$, leading to longer residence times prior to detachment or higher attachment rates for larger lattices. Evolved states exhibited treadmilling for all tested values of $\bar{L}^*$, Fig. S3 [25].

Exponential length distributions are less evolvable than treadmilling.—As an alternative to treadmilling, the average target length could also be reached for an exponential length distribution. This occurs when the growth and shrinkage rates at each end are on average independent of the lattice state [16,27]. In this case, the length distribution is given by $P(L) = (1-\alpha)\alpha^L$ for $L = 0, 1, 2, \ldots$, where $\alpha = [k_a^H(+) + k_a^H(-) + k_a^L(+) + k_a^L(-)]/[k_d^H(+) + k_d^H(-) + k_d^L(+) + k_d^L(-)]$. The average length is then $\alpha/(1-\alpha)$, if $\alpha < 1$, such that all possible target average lengths can be reached in this way [16,27]. However, this configuration never evolved in our analysis.

To test whether this state is in principle attainable in our framework, we repeated our analysis in a simplified system

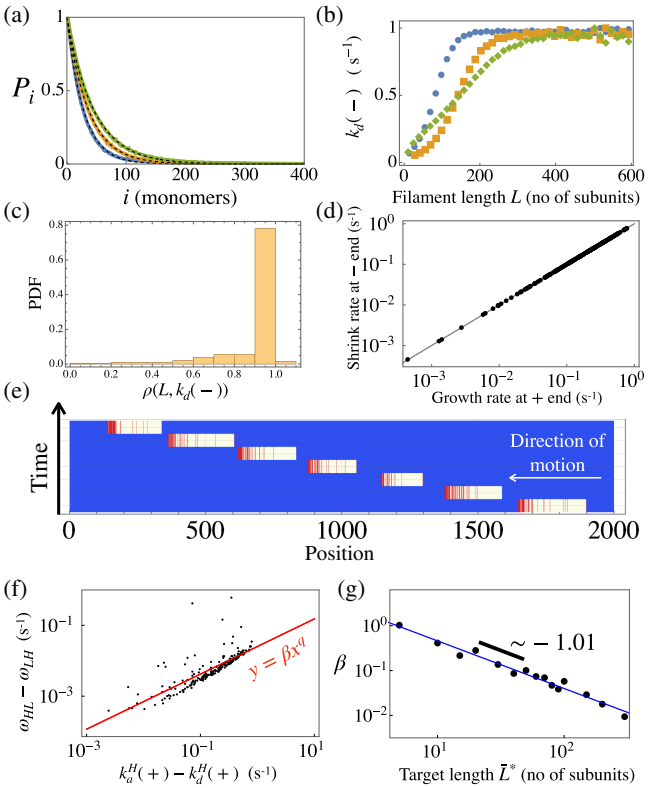

FIG. 3. Lattices exhibit treadmilling at mutation-selection balance. (a) Probability P_i for site i to be in state H in lattices of length $L > i$ (three instances). Dashed black lines show best fit for $y = e^{-x/\lambda}$ that yield $\lambda = 27.8$, 36.5, and 45.3 subunits for the blue, orange, and green curve, respectively. (b) Net detachment rate $k_d(-)$ at the minus end as a function of lattice length [same instances as in (a); all rates and so $k_d(-)$ are cupped at 1 s^{-1}, see Ref. [25]]. (c) Histogram of the Spearman correlation coefficient ρ between lattice length L and $k_d(-)$ for all 204 simulated evolution experiments; ρ close to 1 indicates a monotonic relationship between L and $k_d(-)$. (d) The net shrinkage at the minus end versus net growth rate at plus end for all 204 simulated evolution experiments. Solid line for $y = x$ (correlation coefficient $R^2 = 0.99$). (e) Example of treadmilling dynamics. H and L subunits in red and white, respectively, background in blue. Plus end points to the left. (f) $\omega_{HL} - \omega_{LH}$ versus $k_a^H(+) - k_d^H(+)$. Solid red line for the fit of the form $y = \beta x^q$, where $\beta = 0.03$ and $q = 0.8$. (g) The value of β as a function of the target length, $\bar{L}^*$. All data were obtained in steady state at mutation-selection balance. Individual fits used to obtain β shown in Fig. S2 [25].

with only one subunit state. We introduced mutations in the attachment and detachment rates at the two ends and selected for the target length as before. Under these conditions, the lattice average length consistently converged to the target length and an exponential length distribution emerged, Figs. 4(a) and 4(b). The evolved lattices grew and shrank independently at both ends and did not exhibit directed motion, Fig. 4(c).

From these simplified dynamics we can infer why exponential distributions did not evolve in our full

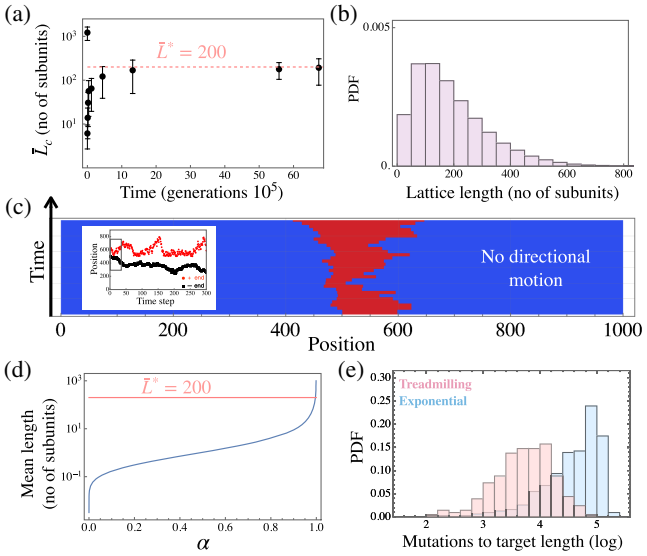

FIG. 4. Exponential length distributions are less evolvable than treadmilling. (a) Example of current mean length, $\bar{L}_c$, in steady state versus evolutionary generation time. Bars indicate standard deviation of the steady-state length distribution. (b) Example steady-state length distribution at mutation-selection balance. (c) Typical example of lattice dynamics in space at mutation-selection balance. Inset shows zoomed in position of the plus (red) and minus (black) ends of the lattice over longer time periods. Gray rectangle indicates a time period over which the kymograph is plotted. (d) Mean lattice length as a function of $\alpha = \{[k_a(+) + k_a(-)]/[k_d(+) + k_d(-)]\}$, where $k_a(+)$ is the attachment rate of the single subunit considered at the plus end and similarly for the other rates. (e) PDFs of the number of mutations required to reach the target length in full (pink) and simplified (blue) simulations.

simulations. Exponential distributions can yield lattice lengths with $\bar{L}^* \gtrsim 10$ only when α is close to 1, i.e., when the attachment and detachment rates are closely matched, Fig. 4(d). Furthermore, the mean length of an exponential distribution diverges as α approaches 1, Fig. 4(d). Therefore, the mean lattice length is extremely sensitive to mutations that change the value of α suggesting that exponential distributions may be challenging to fine-tune by evolution. Accordingly, the total number of mutations needed to reach the target average length through treadmilling in the full simulations was typically more than an order of magnitude smaller than in the simplified simulations, Fig. 4(e).

To explore the sensitivity of the lattice mean length on parameters in treadmilling versus exponential distributions, we introduced small perturbations in the attachment rates in evolved parameter sets. As expected, a substantially larger divergence away from the target length for the same shifts in the rates is seen in the exponential distribution compared to that obtained for treadmilling, Fig. S4 [25].

Conclusion.—We computationally evolved molecular building blocks into machines that can perform work by selecting for a single physical feature. Physical constraints are recognised as central players in evolution [28,29], but how such constraints lead to new forms and functionalities at the molecular level is poorly understood. This lack in understanding is partly due to the challenge in designing appropriate evolution experiments and the lack of suitable theoretical frameworks that could identify important factors in driving the *de novo* evolution of complex and composite functions. The work presented here is a step forward in that direction and could guide experimental endeavours to study the evolutionary potential of molecular self-assembly or the design of biomolecules that can exhibit directional motion and perform work.

We do not directly address the evolutionary path through which treadmilling may have emerged in existing polymers, but instead use treadmilling as a specific example of a simple molecular motor. Therefore, comparison of the evolved rates in our analysis to those relevant to extant treadmilling polymers is beyond the scope of this work.

Physical aspects have been included in evolutionary algorithms to organize contractile and passive blocks into clusters that operate functions [30]. This approach has also been exploited to elucidate design rules underlying nanoparticle uptake by cells [31]. Our findings extend these works by suggesting that physical constraints governing molecular self-assembly can, in principle, lead to the *de novo* evolution of complex functions and molecular machines under simple selection pressures.

The code used for the evolution algorithm in this work is available at [32].

Z. H. was supported by the Francis Crick Institute, which receives its core funding from Cancer Research UK; the UK Medical Research Council, and Wellcome Trust. We thank Charlotte Aumeier, Jean-Pierre Eckmann, Marcos Gonzalez-Gaitan, and Michel Milinkovic for comments.

*Corresponding author: zena.hadjivasiliou@ucl.ac.uk
†Corresponding author: karsten.kruse@unige.ch

[1] A. R. Leman and E. Noguchi, The replication fork: Understanding the eukaryotic replication machinery and the challenges to genome duplication, Genes **4**, 1 (2013).
[2] J. L. Ross, M. Y. Ali, and D. M. Warshaw, Cargo transport: Molecular motors navigate a complex cytoskeleton, Curr. Opin. Cell Biol. **20**, 41 (2008).
[3] F. Jülicher, A. Ajdari, and J. Prost, Modeling molecular motors, Rev. Mod. Phys. **69**, 1269 (1997).
[4] C. Darwin, *On the Origin of Species by Means of Natural Selection* (Murray, London, 1859).
[5] D. Nilsson, The evolution of eyes and visually guided behaviour, Philos. Trans. R. Soc. B, Biol. Sci. **364**, 2833 (2009).
[6] D. Ortega and M. Beeby, How did the archaellum get its rotation?, Front. Microbiol. **12**, 803720 (2022).
[7] A. Wegner, Head to tail polymerization of actin, J. Mol. Biol. **108**, 139 (1976).

[8] R. A. Walker, E. T. O'Brien, N. K. Pryer, M. F. Soboeiro, W. A. Voter, H. P. Erickson, and E. D. Salmon, Dynamic instability of individual microtubules analyzed by video light microscopy: Rate constants and transition frequencies, J. Cell Biol. **107**, 1437 (1988).

[9] V. I. Rodionov and G. G. Borisy, Microtubule treadmilling *in vivo*, Science **275**, 215 (1997).

[10] R. A. Larsen, C. Cusumano, A. Fujioka, G. Lim-Fong, P. Patterson, and J. Pogliano, Treadmilling of a prokaryotic tubulin-like protein, TubZ, required for plasmid stability in Bacillus thuringiensis, Genes Dev. **21**, 1340 (2007).

[11] M. Toro-Nahuelpan, F. D. Müller, S. Klumpp, J. M. Plitzko, M. Bramkamp, and D. Schüler, Segregation of prokaryotic magnetosomes organelles is driven by treadmilling of a dynamic actin-like MamK filament, BMC Biol. **14**, 88 (2016).

[12] A. W. Bisson-Filho, Y.-P. Hsu, G. R. Squyres, E. Kuru, F. Wu, C. Jukes, Y. Sun, C. Dekker, S. Holden, M. S. VanNieuwenhze, Y. V. Brun, and E. C. Garner, Treadmilling by FtsZ filaments drives peptidoglycan synthesis and bacterial cell division, Science **355**, 739 (2017).

[13] X. Yang, Z. Lyu, A. Miguel, R. McQuillen, K. C. Huang, and J. Xiao, GTPase activity–coupled treadmilling of the bacterial tubulin FtsZ organizes septal cell wall synthesis, Science **355**, 744 (2017).

[14] J. W. McCausland, X. Yang, G. R. Squyres, Z. Lyu, K. E. Bruce, M. M. Lamanna, B. Söderström, E. C. Garner, M. E. Winkler, J. Xiao, and J. Liu, Treadmilling FtsZ polymers drive the directional movement of sPG-synthesis enzymes via a Brownian ratchet mechanism, Nat. Commun. **12**, 609 (2021).

[15] K. D. Whitley, C. Jukes, N. Tregidgo, E. Karinou, P. Almada, Y. Cesbron, R. Henriques, C. Dekker, and S. Holden, FtsZ treadmilling is essential for Z-ring condensation and septal constriction initiation in Bacillus subtilis cell division, Nat. Commun. **12**, 2448 (2021).

[16] C. Erlenkämper and K. Kruse, Treadmilling and length distributions of active polar filaments, J. Chem. Phys. **139**, 164907 (2013).

[17] E. B. Stukalin and A. B. Kolomeisky, ATP hydrolysis stimulates large length fluctuations in single actin filaments., Biophys. J. **90**, 2673 (2006).

[18] X. Li, J. Kierfeld, and R. Lipowsky, Actin polymerization and depolymerization coupled to cooperative hydrolysis, Phys. Rev. Lett. **103**, 048102 (2009).

[19] P. Ranjith, K. Mallick, J.-F. Joanny, and D. Lacoste, Role of ATP-hydrolysis in the dynamics of a single actin filament, Biophys. J. **98**, 1418 (2010).

[20] W. Kabsch, H. G. Mannherz, D. Suck, E. F. Pai, and K. C. Holmes, Atomic structure of the actin: DNase I complex., Nature (London) **347**, 37 (1990).

[21] A. A. Hyman, D. Chrétien, I. Arnal, and R. H. Wade, Structural changes accompanying GTP hydrolysis in microtubules: Information from a slowly hydrolyzable analogue guanylyl-(alpha,beta)-methylene-diphosphonate, J. Cell Biol. **128**, 117 (1995).

[22] F. M. Ruiz, S. Huecas, A. Santos-Aledo, E. A. Prim, J. M. Andreu, and C. Fernández-Tornero, FtsZ filament structures in different nucleotide states reveal the mechanism of assembly dynamics, PLoS Biol. **20**, e3001497 (2022).

[23] T. D. Pollard and G. G. Borisy, Cellular motility driven by assembly and disassembly of actin filaments, Cell **112**, 453 (2003).

[24] A. Brännström, J. Johansson, and N. von Festenberg, The Hitchhiker's guide to adaptive dynamics, Games **4**, 304 (2013).

[25] See Supplemental Material at http://link.aps.org/supplemental/10.1103/PhysRevLett.131.208402 for details on the evolution algorithm, calculations, numerical methods, and Supplementary Figures S1–S4.

[26] T. J. Attard, J. P. I. Welburn, and J. A. Marsh, Understanding molecular mechanisms and predicting phenotypic effects of pathogenic tubulin mutations, PLoS Comput. Biol. **18**, e1010611 (2022).

[27] L. Mohapatra, B. L. Goode, P. Jelenkovic, R. Phillips, and J. Kondev, Design principles of length control of cytoskeletal structures, Annu. Rev. Biophys. **45**, 85 (2016).

[28] D. W. Thompson, *On Growth and Form*, edited by J. T. Bonner, Canto (Cambridge University Press, Cambridge, England, 1992).

[29] C. S. Cockell, *The Equations of Life: How Physics Shapes Evolution* (Basic Books, New York, 2018).

[30] S. Kriegman, D. Blackiston, M. Levin, and J. Bongard, A scalable pipeline for designing reconfigurable organisms, Proc. Natl. Acad. Sci. U.S.A. **117**, 1853 (2020).

[31] J. C. Forster, J. Krausser, M. R. Vuyyuru, B. Baum, and A. Šarić, Exploring the design rules for efficient membrane-reshaping nanostructures, Phys. Rev. Lett. **125**, 228101 (2020).

[32] The code used in this work has been written on c/c++ and can be accessed freely at: https://github.com/zenah12/TreadmillingEvo.